CO_2 absorption/desorption in aqueous single and novel hybrid solvents of glycerol and monoethanolamine in a pilot-scale packed bed column

Somayeh Mirzaei[a,b], *Ahmad Shamiri*[c], *Mohamed Kheireddine Aroua*[d,e*]

a. Chemical Engineering Department, Faculty of Engineering, University Malaya, 50603 Kuala Lumpur, Malaysia

b. Chemical Engineering Department, Faculty of Engineering, National Tsing Hua University (NTHU), Hsinchu 30013, Taiwan

c. Reliability and Improvement Department, Dyno Nobel, 667 Goonyella Road, Moranbah QLD 4744, Australia

d. Research Centre for Nano-Materials and Energy Technology (RCNMET), School of Science and Technology, Sunway University, Bandar Sunway, 47500 Petaling Jaya, Malaysia

e. Department of Engineering, Lancaster University, Lancaster, LA1 4YW, UK

KEYWORDS: CO_2 absorption; glycerol; MEA; packed column; simulation

* Corresponding author. Tel.: +603-7491 8622 ext 7166; Fax: +603-5635 8630

E-mail address: kheireddinea@sunway.edu.my (M.K. Aroua).

ABSTRACT

CO_2 removal from mixed CO_2–N_2 gas was investigated by using aqueous solutions of monoethanolamine (MEA) (10 wt%), glycerol (10 wt%), and a mixture of MEA (10 wt%)–glycerol (10 wt%) in a pilot-scale packed column. Aspen Plus simulator was employed to simulate the CO_2–MEA–glycerol process using a rate-based model. Then, the experimental data of pilot-scale columns were applied to validate the simulation results. The lowest and highest rich CO_2 loadings for the MEA solvent were measured in 3.65% and 13.9% mol CO_2/mol MEA with 1.4 and 3.9 L/min gas flow rates, respectively. In comparison to CO_2–MEA system, the lowest and highest rich CO_2 loadings for CO_2–MEA–glycerol system increased by 42.2% and 14.8%, respectively under the same conditions. The values of CO_2 loadings predicted by the simulation were in concordance with the experimental values. Results suggested that the hybrid MEA–glycerol solution had better CO_2 absorption performance than the aqueous MEA solution.

1. INTRODUCTION

Carbon dioxide (CO_2) removal techniques have been extensively used in various parts of industries, for example, CO_2 capture from flue gas and natural gas purification.[1, 2] Given the international aims to decrease greenhouse gas discharges, CO_2 capture from flue gas has attracted growing consideration in the last few years.[3-5] One efficient method for CO_2 capture is the use of aqueous alkanolamine solutions or their mixtures.[4, 6, 7] Monoethanolamine, diethanolamine, and N-methyldiethanolamine[8, 9] are conventional chemical absorbents.[1, 4, 10, 11] Piperazine is commonly used as a blend with other amines because its absorption capacity for CO_2 and absorption rate[7, 8] are approximately twice than those of MEA and its energy requirements are approximately 15% less than those of MEA.[12] Ionic liquids (ILs) can operate as

independent solvents[1, 13]and can also be consumed as activators for aqueous amines or other ILs.[14] Li et al. reported that the removal of SO_x, NO_x, and mercury from flue gas along with CO_2 capture is an advantage of the ammonia (NH_3) process over conventional amines.[7] Nevertheless, the vapor pressure of NH_3 is high, resulting in considerable solvent losses.[12] The current industry standard is the application of 30 wt% MEA aqueous solution for CO_2 absorption/desorption.[15] MEA is inexpensive compared with other amines and soluble in water at all concentrations. It has a high absorbing capacity on a mass basis and high reactivity. MEA reacts quickly with CO_2. Notwithstanding new solvents, MEA remains the most commonly used amine for CO_2 capture.[2, 16-18]

Another alternative for CO_2 capture is physical absorption with the less energy-intensive regeneration of solvent. Physical absorption is effective for a flue gas stream with high CO_2 partial pressure, typically more than 15 vol%. [19] Recently, research on CO_2 capture has focused on enhancing performance by hybrid solutions, which are formed by blending chemical and physical solvents.[2, 15, 20, 21]

The production of biodiesel generates approximately 10% of glycerol by volume.[22, 23] Therefore, finding alternative applications for excess glycerol is necessary.[24-26] The addition of glycerol to MEA[27]and methanol mixtures improves absorption capacity and decreases regeneration energy compared with aqueous MEA solution. However, cyclic absorption capacity decreases after the addition of glycerol.[28] Shamiri et al.[27] showed that the solubility of the MEA solution increased by adding glycerol up to a level of 10% at lower pressures. They confirmed that the solvent is suitable for the absorption of CO_2 under low pressures (below 1000 kPa) and can be applied in low-pressure CO_2 absorption processes such as post-combustion CO_2 capture.

The addition of glycerol to ammonia solution reduces vaporization and improves CO_2 absorption.[11] Glycerol has the highest molar solubility for CO_2 and the maximum solubility for nitrogen (N_2) compared with polyethylene glycol (PEG) 300, PEG 600, or poly(ethylenimine).[29] The volatile nature of amines causes serious environmental drawbacks due to the drastic loss of solvents into the gas stream. [17, 30] The high amount of energy needed for the regeneration of solvent in stripping columns increases operating costs.[3, 4, 15, 31] The solvent regeneration and energy requirement of physical absorption are simpler and lower, respectively, than those of chemical absorption. [32]

Amines undergo thermal degradation in regeneration and oxidative degradation when oxygen is present in the flue gas stream. The effects of amine degradation include a reduction in CO_2 loading capacity, foaming, fouling, and increased viscosity. [33, 34] Moreover, the vapor pressure of MEA is high and leads to considerable solvent loss through evaporation and serious environmental drawbacks. [29] To overcome the drawbacks of MEA solvent, researchers have studied the mixture of amines and physical solvents [15, 35] as chemical solvents are corrosive in nature.[36]

Recently, glycerol, a novel solvent, has been studied for its application in CO_2 capture. It is ecofriendly, stable, and liquid at slight vapor pressure points. [37] Glycerol is abundantly available as a by-product of biodiesel production. [22, 26, 38] Thus, it is inexpensive [22] and biodegradable. Glycerol is colorless and odorless. Moreover, it has a high boiling point, and it is nonvolatile at atmospheric pressure. [27, 29] Furthermore, the high viscosity of pure glycerol in glycerol aqueous solutions can be reduced by increasing the amount of water and temperature. The solubility of CO_2 in glycerol is greater than that in water. [29, 39] Therefore, the application of glycerol can decrease the use of toxic chemical solvents. Most studies on glycerol and hybrid solution

systems have been performed on a laboratory scale. To the best of our knowledge, data in the open literature for CO_2 absorption using MEA–glycerol solvent in a pilot-scale packed column are unavailable. In this study, the capability of glycerol to remove CO_2 from a gas mixture of CO_2 (15 v%) and N_2 (85 v%) using a packed column is investigated. This aim is precisely achieved through the following:

First, the performance of CO_2 absorption and CO_2 removal using mixtures of MEA–glycerol aqueous solution, MEA aqueous solution, and glycerol aqueous solution in pilot-scale packed columns is evaluated. Then, CO_2 absorption and separation columns are simulated in Aspen Plus using an aqueous blend of MEA–glycerol, and the simulation results are validated with experimental work.

2. METHODOLOGY

The procedure used in this work for the experimental and simulation studies of packed bed columns is shown in Figure 1.

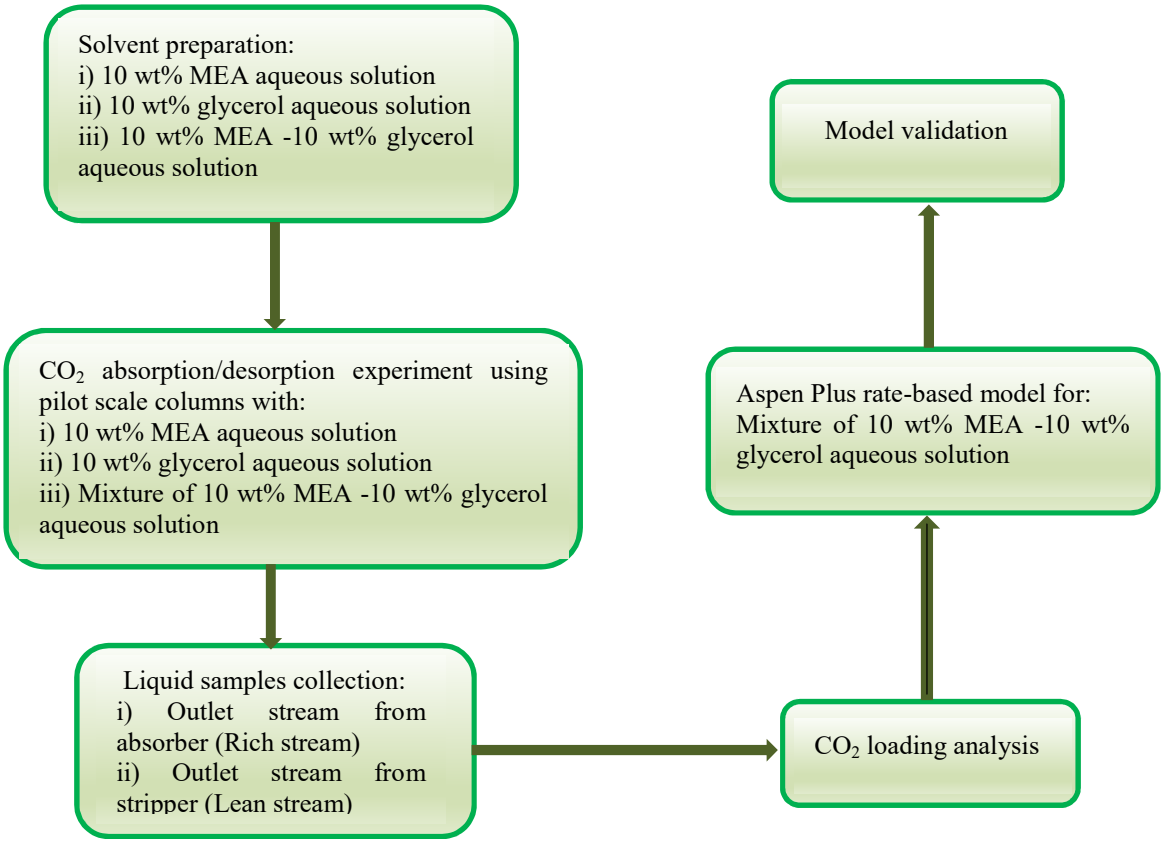

Figure 1. Methodology used in this study.

2.1. Materials

MEA (purity>98%) and glycerol (purity>99.8%) were supplied by R&M Chemicals and used as purchased without further purification. Barium chloride ($BaCl_2$) solution with a concentration of 0.3 M was prepared by mixing barium chloride dihydrate ($BaCl_2 \cdot 2H_2O$) (purity>99% obtained from R&M Chemicals) with distilled water. Sodium hydroxide (NaOH) and hydrochloric acid (HCl) with concentrations of 0.1 N were used as received from R&M Chemicals. Distilled water was provided by a Favorit Water Still W4L water purification system. This system provides distilled water produced through a power input by a chromium-plated heater housed in a

horizontal glass boiler. Mixed CO_2–N_2 gas with a composition of 15 v% CO_2 and 85 v% N_2 was supplied by Linde, a special gas center in Malaysia.

2.2. Pilot-scale absorption/desorption unit

A pilot-scale absorption/desorption unit containing two separate but interconnected packed columns was employed for CO_2 scrubbing and solvent regeneration (Figure 2). The simple schematic of pilot-scale unit is shown in Figure 3.

The gas contacts with the liquid counter-currently inside the packed column. The unit continuously operates at atmospheric pressure. The absorber and stripper columns are borosilicate glass and stainless steel filled with glass Raschig rings. Sampling points for composition analysis are provided for liquid streams. The mixed CO_2–N_2 gas is fed into the bottom of a packed absorption column, whereas the solvent enters from the top of the column through a centrifugal pump. CO_2 is transferred from the gas mixture into solvent when gas and liquid come into contact. Solvent comprising CO_2 (rich solvent) can be stripped in the packed desorption column. The CO_2-rich solvent is heated before entering the desorption column to decrease the solubility of CO_2 in the solvent. The desorber removes CO_2 by increasing the temperature of the solution. Tables 1 and 2 indicate the characteristics of the absorption and desorption columns and the used packings, respectively.

Figure 2. Pilot-scale CO_2 absorption/desorption unit in the University of Malaya.

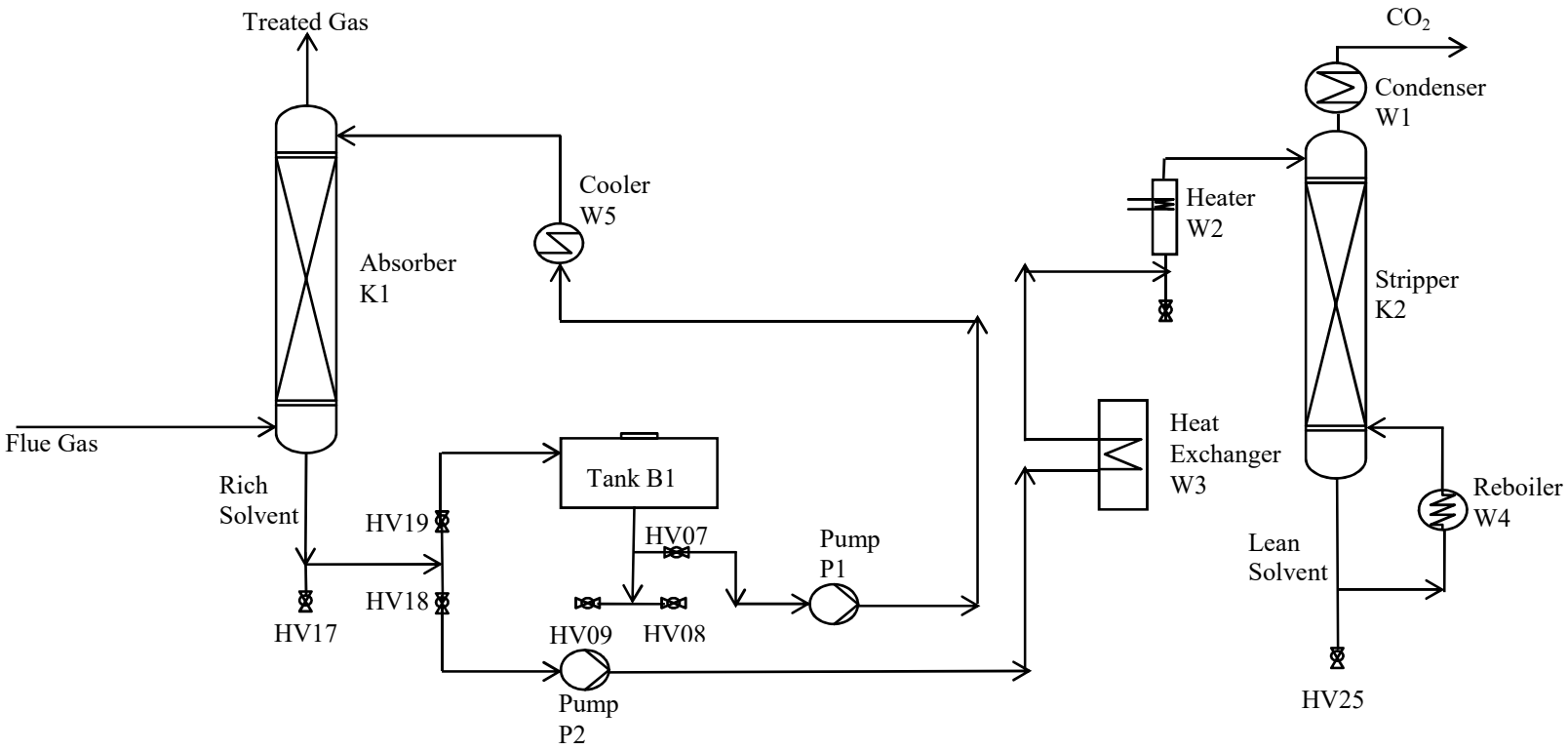

Figure 3. Simple schematic of pilot-scale CO_2 absorption/desorption unit in the University of Malaya.

Table 1. Characteristics of absorber and stripper columns.

	Specification
Column type	packed
Column internal diameter(mm)	80
Effective packing height(m)	1.5
Packing type	Raschig rings
Nominal packing size (mm)	8

Table 2. Physical characteristics of Raschig rings.[40]

Material	Size (mm)	Geometric surface area (cm^2/cm^3)	Void fraction (cm^3/cm^3)	Packing factor (cm^{-1})
glass	8	4.61	0.76	10.50

2.3. CO_2 removal operation

In this study, CO_2 removal involved three types of aqueous solutions, including MEA (10 wt%), glycerol (10 wt%), and MEA (10 wt%)–glycerol (10 wt%). These concentrations were selected on the basis of the discussions in our previous work.[32]

Fifty liters of each aqueous solution was prepared on the basis of volume concentrations using the distilled water. Fourteen experimental runs were performed in the absorption/desorption unit at five different gas flow rates (1.4, 1.7, 2.9, 3.3, and 3.9 L/min) using aqueous solutions of MEA, glycerol, and MEA–glycerol. The solvent was fed into the absorption column with a

temperature of approximately 29.4 °C and a 0.7 L/min flow rate. The CO_2–N_2 gas with a composition of 15 v% CO_2 and 85 v% N_2 was entered into the absorber. Gas entering the absorber counter-currently contacted with the aqueous solvent. CO_2 was absorbed into the aqueous solvent to form a rich solvent that was then sent through a heat exchanger. In the stripper, heat was provided in the reboiler by increasing the temperature using an oil bath. The liberated CO_2 and the hot, lean solvent left the stripper from the top and bottom of the column. Liquid samples were collected in the absorber outlet stream (rich solvent) and in the stripper outlet stream (lean solvent) to be checked for CO_2 loadings using the titration method. The CO_2 absorption/desorption system was kept under steady-state conditions for almost 5 min before liquid sampling. After each sampling, a new CO_2 absorption process was attempted by varying the gas flow rate. In addition to the liquid sampling, instantaneous online measurements, such as temperatures, flow rates, and liquid levels, were recorded using SCADA. Table 3 shows the experimental conditions of CO_2 removal in this study. CO_2 loading was used as the indicator to evaluate the performance of solvents. For the MEA–glycerol solution, CO_2 loading was stated as moles of CO_2/mole alkalinity. Given that glycerol is neutral in the litmus test,[41] the number of nitrogen atoms on amine defines the alkalinity of the solution.[42] Moreover, MEA has only one nitrogen atom. Therefore, the CO_2 loading indicator is calculated as follows:

For mixture of MEA–glycerol solution: CO_2 loading = n CO_2/[(1) n $_{MEA}$] (1)

For MEA solution: CO_2 loading = mol CO_2/mol MEA (2)

For glycerol solution: CO_2 loading = mol CO_2/mol glycerol (3)

Table 3. Experimental conditions for CO_2 absorption in the packed column.

Operating parameter	Gas	Amine solution	Mixed solvent	Glycerol solution
Temperature (℃)	30	29.4	29.4	29.4
Pressure (barg)	0.11	0.11	0.11	0.11
	Vol frac.	Mass frac.	Mass frac.	Mass frac.
H_2O	-	0.9	0.8	0.9
CO_2	0.15	-	-	-
MEA	-	0.1	0.1	-
N_2	0.85	-	-	-
Glycerol	-	-	0.1	0.1

3. SIMULATION STUDY BASED ON EXPERIMENTAL WORK

The CO_2 removal process for the CO_2–MEA–glycerol system was simulated on the basis of a rigorous rate-based model, which was implemented in the process simulator Aspen Plus v7.3, and simulation results were validated using the experimental data of pilot-scale columns. The CO_2–MEA–glycerol system is an electrolyte system wherein the nonideality of the liquid phase must be considered. ENRTL-RK is adopted as thermodynamic property in the simulations

because it is an extended asymmetric ENRTL model for mixed electrolyte systems.[43] All chemical reactions, equilibrium constants, kinetic parameters for the reactions, and Henry's constants for this model were from Mirzaei et al.[32] The average absolute deviation percent (%AAD) (Equation 4) was applied to compute the deviation between the simulation and experimental results. N, Y_{Sim}, and Y_{Exp} are defined as the number of process variables, simulated, and experimental data, respectively.

$$\%AAD = \frac{100}{N}\sum_{i}^{N}\frac{\left|Y_i^{sim} - Y_i^{Exp}\right|}{Y_i^{Exp}} \quad (4)$$

3.1. Absorber simulation

The absorber column was modeled using RadFrac packed column, and 20 stages were used to represent the packing. The absorber simulation flowsheet is illustrated in Figure 4. Pack rating is applied in Aspen Plus rate-based simulations to specify the column diameter and packing height. The characteristics of absorption column and feed conditions for the MEA–glycerol solvent were defined on the basis of Tables 1–3. The absorber performance is modeled by combining the equilibrium and kinetic reactions of 5–11[32]:

$$Equlibrium \quad MEAH^+ + H_2O \leftrightarrow MEA + H_3O^+ \quad (5)$$

$$Equlibrium \quad HCO_3^- + H_2O \leftrightarrow H_3O^+ + CO_3^{2-} \quad (6)$$

$$Equlibrium \quad 2H_2O \leftrightarrow H_3O^+ + OH^- \quad (7)$$

$$Kinetic \quad MEA + CO_2 + H_2O \rightarrow MEACOO^- + H_3O^+ \quad (8)$$

$$Kinetic \quad MEACOO^- + H_3O^+ \rightarrow MEA + H_2O + CO_2 \quad (9)$$

$$Kinetic \quad CO_2 + OH^- \rightarrow HCO_3^- \quad (10)$$

$$Kinetic \quad HCO_3^- \rightarrow CO_2 + OH^- \quad (11)$$

Mass transfer coefficients and the interfacial area for the packing are calculated by Aspen Plus using the correlation of Bravo and Fair.[44] Bravo and Fair correlation predicts mass transfer coefficients and interfacial area for random packings. Although they use the same expressions as the Onda correlation for the mass transfer coefficients, the modified Reynolds number used in calculating the liquid phase mass transfer coefficient is based on effective surface area rather than wetted surface area.[45] The correlation of heat transfer is selected from Chilton and Colburn.[46]

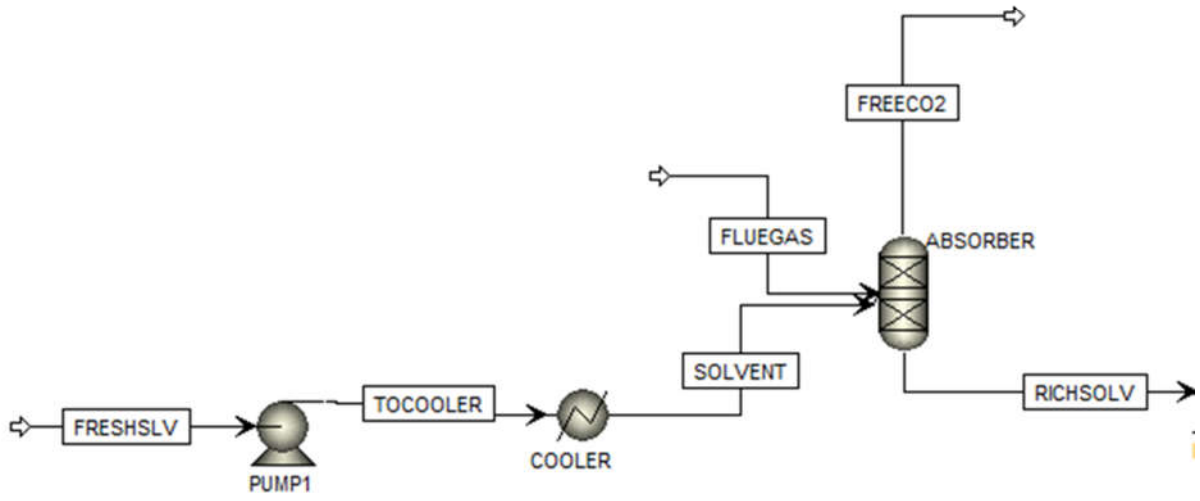

Figure 4. Schematic of the absorption process.

3.2. Stripper simulation

The stripper column was simulated using a RadFrac column comprising 20 stages with a partial-vapor condenser (stage 1) and a kettle reboiler at the bottom (stage 20). The characteristics of the stripper column in this simulation study were specified on the basis of Tables 1 and 2. The temperature, flow rate, and composition of the stripper feed obtained from absorber simulations were introduced into the model. The stripper simulation flowsheet is shown in Figure 5. The

correlation of Onda et al.[47] is used in Aspen Plus as the mass transfer coefficient method and the interfacial area method. Heat transfer coefficients were calculated by Aspen Plus using the correlation of Chilton and Colburn.[46] Table 4 shows the suggested correlations for interfacial area, mass transfer, and heat transfer coefficients in this study.

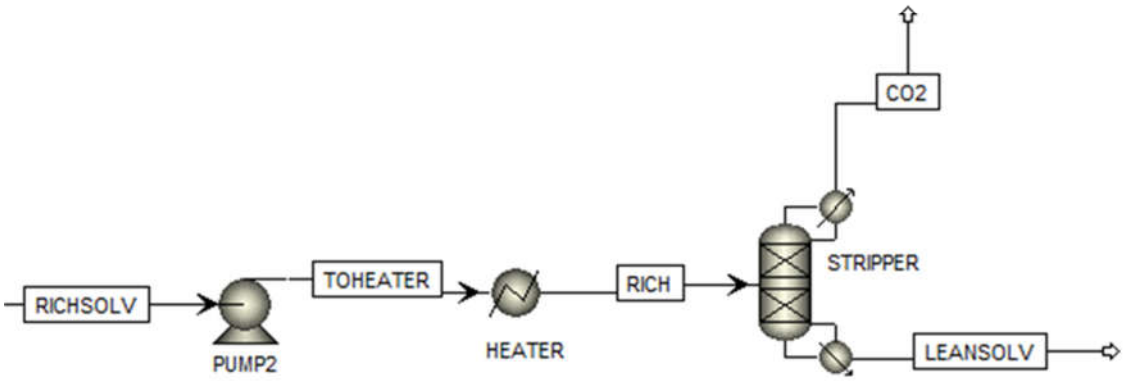

Figure 5. Schematic of the desorption process.

Table 4. Proposed correlations of mass transfer, interfacial area, and heat transfer coefficients in the simulation.

Correlation	Reference
$k_{i,k}^{L} = 0.0051\left(\acute{Re}_L\right)^{0.667} Sc_{L_{j,k}}^{-0.5}\left(a_p d_p\right)^{0.4}\left(\frac{\mu^L g}{\rho_t^L}\right)^{0.333}$	44
$k_{i,k}^{V} = 2Re_V^{0.7} Sc_{V,i,k}^{0.333} a_p D_{i,k}^{V}\left(a_p d_p\right)^{-2} \;\; if\; d_p < 0.015\; m$ $k_{i,k}^{V} = 5.23Re_V^{0.7} Sc_{V_{j,k}}^{0.333} a_p D_{i,k}^{V}\left(a_p d_p\right)^{-2} \;\; if\; d_p > 0.015\; m$	44
$a^I = \; a_e A_t h_p$ $a_e = 19.78 a_p (Ca_L Re_V)^{0.392}\sigma^{0.5}/h_p^{0.4}$	44
$a^I = a_w A_t h_p$ $a_w = a_p\left[1 - exp\left(-1.45\left(\frac{\sigma_c}{\sigma}\right)^{0.75} Re_L^{0.1} Fr_L^{-0.05} We_L^{0.2}\right)\right]$	47
$h^L = \bar{k}^L \bar{\rho}^L C_P^L \left(\frac{\lambda^L}{\bar{\rho}^L C_P^L \bar{D}^L}\right)^{\frac{2}{3}}$ $h^V = \bar{k}^V \bar{\rho}^V C_P^V \left(\frac{\lambda^V}{\bar{\rho}^V C_P^V \bar{D}^V}\right)^{\frac{2}{3}}$	46, 48

4. RESULTS AND DISCUSSION

4.1. Performance of pilot-scale columns

Fourteen experimental runs were conducted with various liquid-to-gas (L/G) flow ratios in the pilot-scale absorber and stripper columns. CO_2 loadings were evaluated only at the outlet stream of the absorber and stripper using the titration method. Table 5 shows the performance of absorber and stripper columns. Based on this experimental study, hybrid solution MEA–glycerol

shows better CO_2 absorption over aqueous MEA solution. As can be seen from Table 5, rich CO_2 loadings in the absorption column for the mixture of MEA–glycerol (runs No. 5–9) are more than those for the MEA solvent and glycerol solvent at the same gas flow rates. Moreover, rich CO_2 loadings for glycerol solution are less than those for MEA solution. These results indicate that glycerol can be applied as a promoter in the MEA process to improve CO_2 absorption capacity.

Table 5. Performance of absorber and stripper columns in this experimental work with solutions of MEA (10 wt%), glycerol (10 wt%), and mixed MEA (10 wt%)–glycerol (10 wt%), 0.7 L/min solvent flow rate, and gas mixture of CO_2 (15 v%)–N_2 (85 v%).

Run	Solvent	Gas flow rate (L/min)	Absorber rich stream CO_2 loading (%)	Stripper lean stream CO_2 loading (%)
1	MEA	1.4	3.65	3.44
2	MEA	1.7	4.56	3.41
3	MEA	2.9	6.75	3.12
4	MEA	3.3	12.6	2.86
5	MEA	3.9	13.9	2.8
5	Mixed	1.4	5.19	4.02
6	Mixed	1.7	5.61	3.89
7	Mixed	2.9	7.59	3.51
8	Mixed	3.3	14.46	3.03

9	Mixed	3.9	15.96	2.96
10	Glycerol	1.4	1.8	1.1
11	Glycerol	1.7	2.1	1.9
12	Glycerol	2.9	5.08	4.09
13	Glycerol	3.3	8.7	3.9
14	Glycerol	3.9	9.8	3.25

Figure 6 shows the influence of gas flow rate on rich CO_2 loadings among MEA solution, glycerol solution, and mixed MEA–glycerol solution in the absorption/desorption unit with 15 vol% CO_2 feed composition. An increase in the gas flow rate increases the amount of CO_2, which is moved between phases. According to the figure, the CO_2 loading increases significantly with gas flow rate of higher than 2.9 L/min. It is mainly due to increasing the CO_2 content in the system, high driving force of CO_2 absorption as well as high CO_2 capture capacity of the solvents. It is noted that the CO_2 loading is steady at gas flow rate of around 3.9 L/min and approaching the saturation limit. As shown in this figure, the rich loading for the mixed MEA–glycerol solution is better than that for the MEA solution. On the other hand, rich CO_2 loading for the glycerol solution is lower than those for the MEA and mixed solution under the same operating conditions. This effect indicates that the CO_2 absorption capacity of the physical solvent is less than that of MEA solution. Reaction 12 describes CO_2 absorption by MEA.

$$CO_2 + 2RNH_2 \leftrightarrow RNHCOO^- + RNH^+ \quad (12)$$

Based on the reaction, 2 moles of MEA absorbs 1 mole of CO_2.[35] As a result, MEA has a maximum loading of 0.5 mole CO_2/mole MEA.[20] On the other hand, the glycerol-rich phase dissolves CO_2 at mole fractions of up to 0.13 over temperature ranges of 40 °C–200 °C and pressures of up to 350 bar. CO_2 solubility in glycerol is superior to that in water.[29, 39] The addition of 5 wt% and 10 wt% glycerol to the MEA solvent improves CO_2 solubility under pressures less than 10 bar, whereas the solubility of CO_2 reduces at 15 wt% and 20 wt% glycerol concentrations.[27] Comparing the absorber rich loadings for MEA solvent and MEA–glycerol solvent in Table 5 and Figure 6 reveals that high loadings are exhibited by the MEA–glycerol solvent. As a result, the addition of glycerol to aqueous MEA solution improves CO_2 absorption capacity.

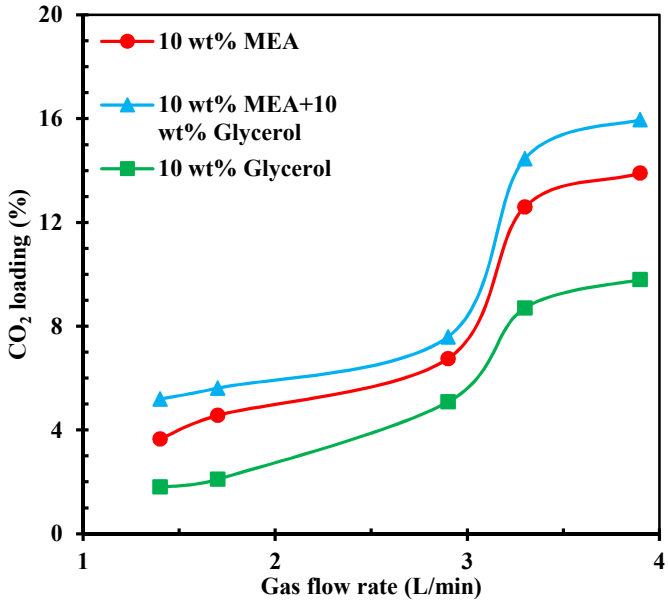

Figure 6. CO_2 loading in rich solvents. Experiments with a) aqueous MEA solution, b) aqueous mixture of MEA–glycerol solution, and c) aqueous glycerol solution.

Figures 7–9 show the rich and lean CO_2 loadings as a function of gas flow rate. The profiles of lean loading profiles are lower than those of rich loadings because of solvent regeneration and CO_2 release in the desorption column. In this work, solvent flow rate is kept constant, whereas

the gas flow rate is varied. Therefore, the difference between the CO_2 loadings of the rich and lean solvents increases. By increasing the gas flow rate, the contact time of the phases is prolonged, and the rich loading is thus increased. The rich loading can considerably affect the absorber outlet temperature. During regeneration, the stripper column was heated to 100 °C. The heat exchanger could increase the temperature to 110 °C.

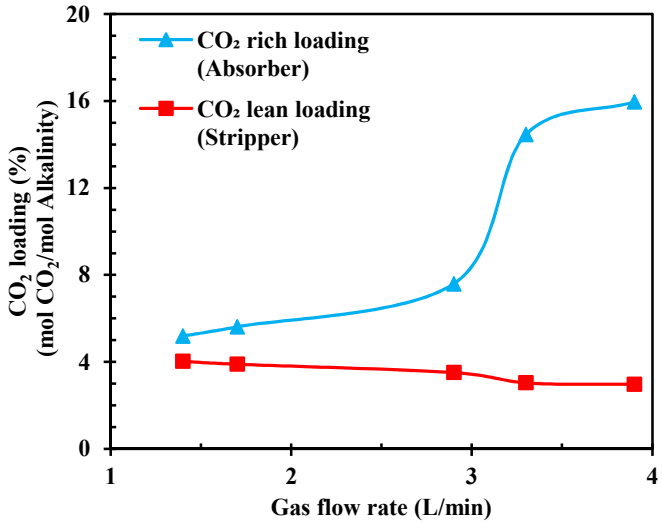

Figure 7. Comparison of CO_2 loadings in the output streams of the absorber and stripper columns. Experiment with the mixed MEA (10 wt%)–glycerol (10 wt%) solution.

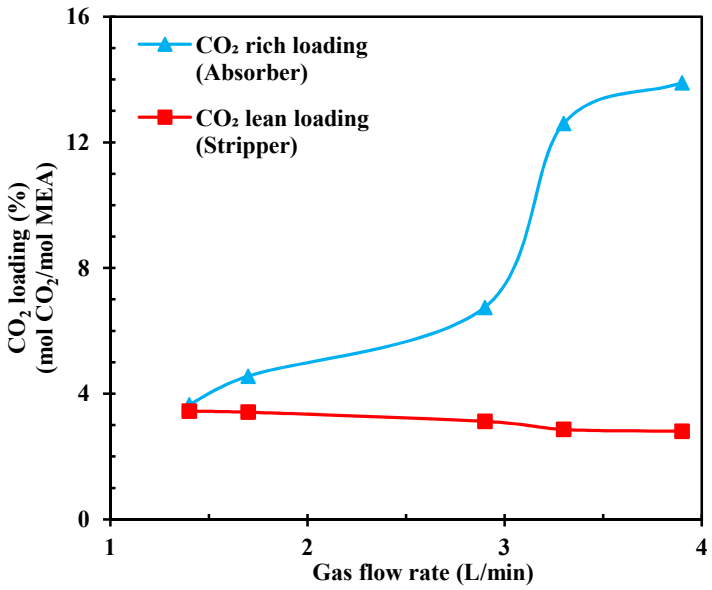

Figure 8. Comparison of CO_2 loadings in the output streams of absorber and stripper columns. Experiment with 10 wt% MEA aqueous solution.

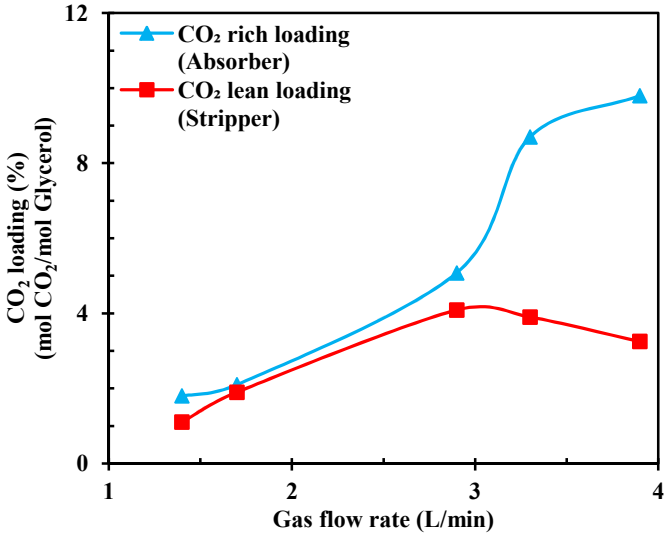

Figure 9. Comparison of CO_2 loading in the output streams of absorber and stripper columns. Experiment with 10 wt% glycerol aqueous solution.

Figures 10–12 illustrate the dependence of absorber outlet liquid temperature on the rich CO_2 loading. The distinct relationship between rich CO_2 loading and temperature confirms the fact that temperature increases by improving the CO_2 loading. As CO_2 loading is increased from 3.65% to 13.9% mole CO_2/mole MEA, temperature increases by 2.3 °C (30 °C–32.3 °C). On the

other hand, the temperature for CO_2 loadings of 5.19%–15.96% mole CO_2/mole alkalinity increases by 0.74 °C (32.01 °C–32.75 °C). However, in the case of the glycerol solvent, when the CO_2 loading is increased from 1.8% to 9.8% mole CO_2/mole glycerol, temperature increases by 0.96 °C (29.85 °C–30.81 °C).

In this experimental study, the solvent is counter-currently contacted by gas comprising CO_2 in the absorber column. The liquid absorbs CO_2 when the solvent is MEA solution and MEA–glycerol solution. As a result of chemical absorption, this process causes the reaction heat and the liquid temperature to increase. Temperature changes for CO_2 loadings obtained from glycerol solvent are low because of the absence of the reaction for this system and because CO_2 dissolves into the glycerol solution.

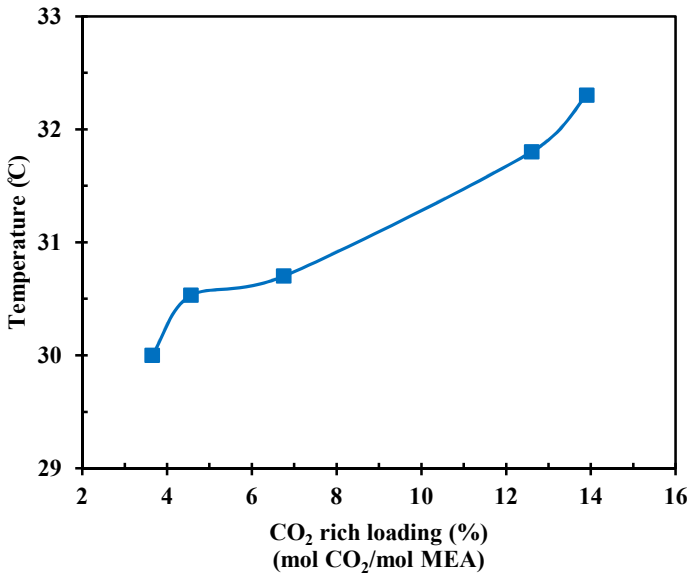

Figure 10. Temperature profile of absorber outlet stream at different CO_2 loadings. Experiment with 10 wt% MEA aqueous solution.

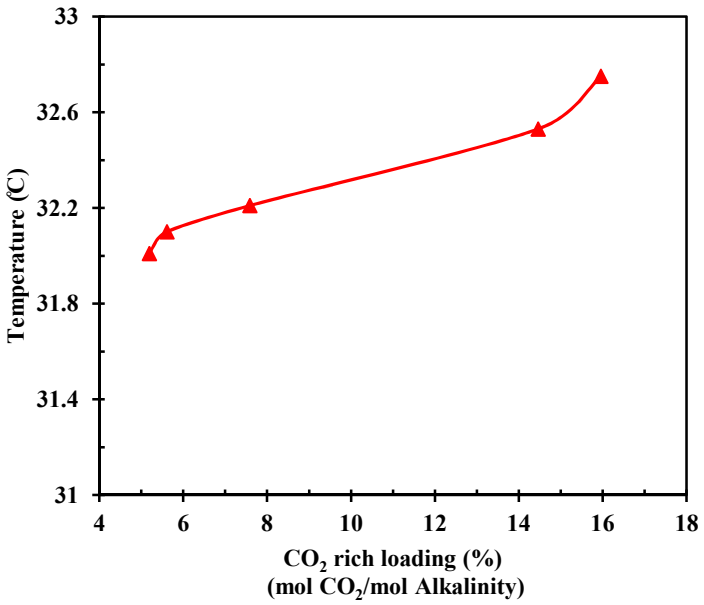

Figure 11. Temperature profile of absorber outlet stream at different CO_2 loadings. Experiment with the mixed MEA (10 wt%)–glycerol (10 wt%) solution.

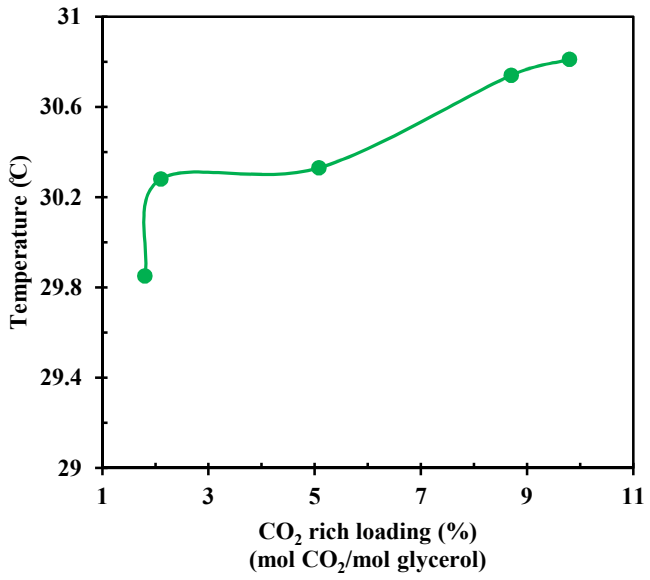

Figure 12. Temperature profile of absorber outlet stream at different CO_2 loadings. Experiment with 10 wt% glycerol aqueous solution.

Comparison of rich stream temperature profiles on the basis of gas flow rates is shown in Figure 13. This figure shows that the temperature of rich loading rises by increasing the gas flow rate. As mentioned, this effect is due to an increase in the gas flow rate that leads to high CO_2 absorption and temperatures. The addition of glycerol to MEA increases the amount of CO_2 absorption. Therefore, the amount of temperature increase for the MEA–glycerol solvent is higher, and temperature profile is located higher than that of MEA and glycerol profiles.

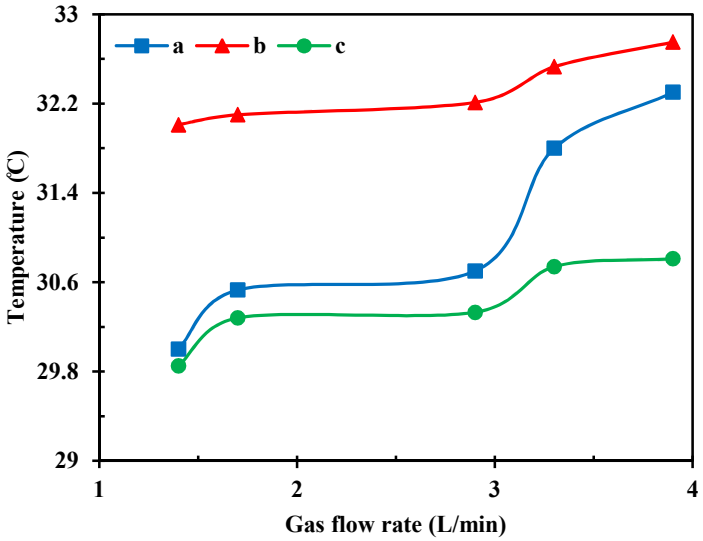

Figure 13. Comparison of the temperature profiles of the absorber outlet stream at different gas flow rates. Experiments with a) aqueous MEA solution, b) aqueous mixture of MEA–glycerol solution, and c) aqueous glycerol solution.

The estimated pH values of different CO_2 loadings are presented in Figure 14. This figure shows that the pH of the aqueous mixture of MEA–glycerol solvent is lower than that of the aqueous MEA solution. This characteristic indicates that MEA–glycerol is more likely to achieve a higher CO_2 loading than the MEA system. As a result, more CO_2 can be absorbed into the MEA–glycerol solution than into the MEA solution at the same gas flow rates. Therefore, glycerol can increase the CO_2 absorption capacity of the MEA as the primary amine. Glycerol is neutral to

litmus, and as shown in the figure, the pH values of all samples collected from CO_2 absorption using glycerol solution are between 7.5 and 8.5.

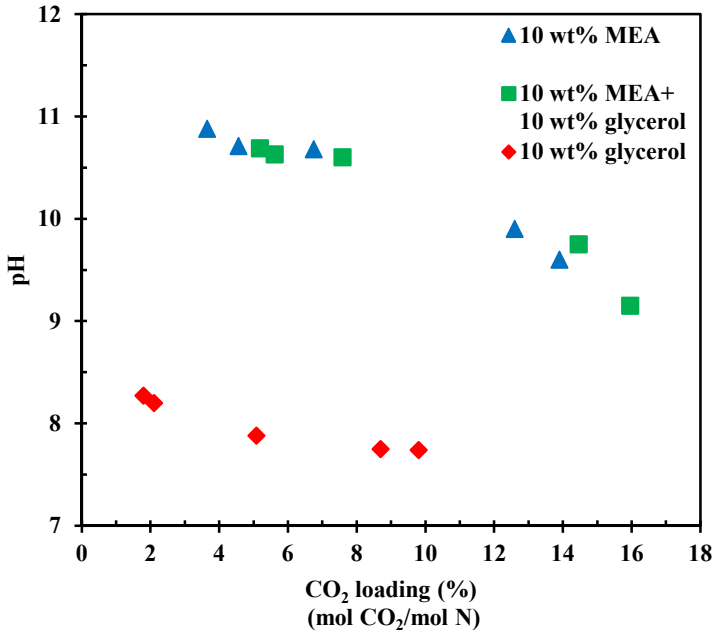

Figure 14. pH profiles of MEA, MEA–glycerol, and glycerol solutions at various CO_2 loadings and constant gas flow rate. N: MEA (mole CO_2/mole MEA); alkalinity (mole CO_2/mole alkalinity) for the mixture of MEA–glycerol; glycerol (mole CO_2/mole glycerol).

4.2. Validation of rate-based modeling

Rate-based modeling was performed for CO_2 absorption using the MEA–glycerol solution, and simulation results were compared with the experimental data of the absorption/desorption unit. %AAD also was calculated using Equation 4. The liquid temperature and CO_2 loadings in the outlet stream from the absorber and stripper are presented on the basis of different gas flow rates.

4.2.1. Absorber simulation

As noted before, glycerol solvent does not chemically react when absorbing CO_2. Instead, the CO_2 dissolves into the glycerol solvent. Table 6 presents the comparison of rich CO_2 loadings

between the experimental and simulation studies for the mixed MEA–glycerol aqueous solution. As shown in the table, the mixed solvent flow rate is kept constant, whereas the gas flow rate rises from 1.4 L/min to 3.9 L/min. An increase in the gas flow rate increases the amount of CO_2 that is moved between phases, and rich CO_2 loading increases. The AAD% values for all gas flow rates are less than 10%. The highest deviation percentage was 9.22% for the 2.9 L/min gas flow rate, whereas the lowest deviation percentage of 0.36% was obtained for the 1.7 L/min gas flow rate. The advantage of adding glycerol to the MEA is that glycerol promotes the amount of CO_2 absorption capacity for MEA–glycerol solution.

Table 6. CO_2 loadings in outlet stream from absorber for CO_2–MEA–glycerol system.

	Rich loading (%) (mole CO_2/mole Alkalinity)		
Gas flow rate (L/min)	Experimental	Simulation	AAD%
1.4	5.19	5.28	1.73
1.7	5.61	5.59	0.36
2.9	7.59	6.89	9.22
3.3	14.46	14.8	2.35
3.9	15.96	16.34	2.38

Figure 15 illustrates rich CO_2 loadings as a function of L/G ratio for MEA–glycerol system. Experimental and simulation study results show that the CO_2 loading increases with a reduction in the L/G ratio. This plot confirms that the prediction of the simulation model matches the experimental data. In this study, gas flow rate increases, whereas the solvent flow rate is stable. Accordingly, the ratio of liquid flow rate to gas flow rate, L/G ratio, changes. Increasing the gas

flow rate to 1.4, 1.7, 2.9, 3.3, and 3.9 L/min decreased the L/G ratio to 0.5, 0.41, 0.24, 0.21, and 0.18, respectively.

As shown in Figure 15, maximum CO_2 loading is at L/G around 0.2 since the gas flow rate is at the highest level and therefore the highest content of CO_2 at this ratio and this contributes to high absorption and CO_2 loading. Furthermore, the CO_2 loading decreases significantly with decreasing gas flow rate or increasing L/G ratio due to decreasing CO_2 content in the system.

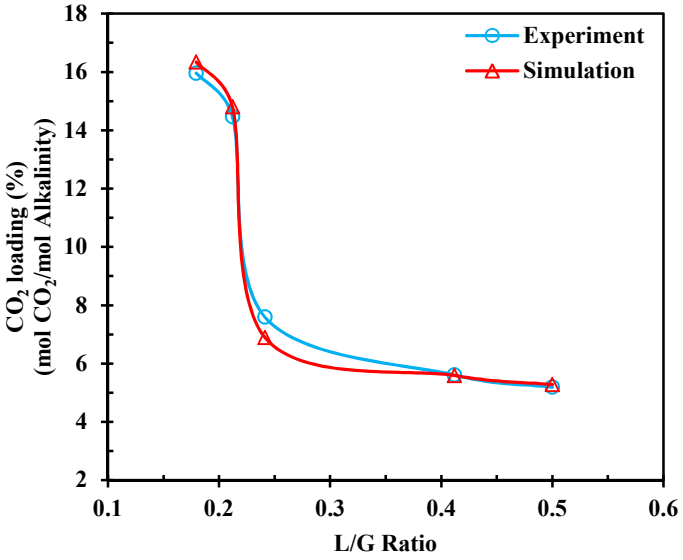

Figure 15. Dependence of the rich CO_2 loading on L/G ratio for mixed MEA–glycerol solvent.

Figure 16 shows the profiles of liquid temperature along the absorber for the MEA–glycerol aqueous solution. The absorber comprises 20 stages wherein the gas input is in the bottom of the column, stage 20, as "Gas-only," and the lean solvent input is in the top of column, stage 1, as "Liquid-only."

The CO2–MEA reaction is exothermic. The temperature in the absorber rises given that this reaction generates energy. Reaction 8 is one of the most important reactions that occur in the

absorber column, indicating that the reaction between MEA and CO_2 produces carbamate ($MEACOO^-$):

$$MEA + CO_2 + H_2O \rightarrow MEACOO^- + H_3O^+ \quad (8)$$

As can be seen from Figure 16, high gas flow rates change the temperatures in the absorber to the upper values. When the gas flow rate rises, the released CO_2 absorption heat increases and improves absorber temperature. The heat of CO_2 reaction with MEA produces a temperature bulge in the column.

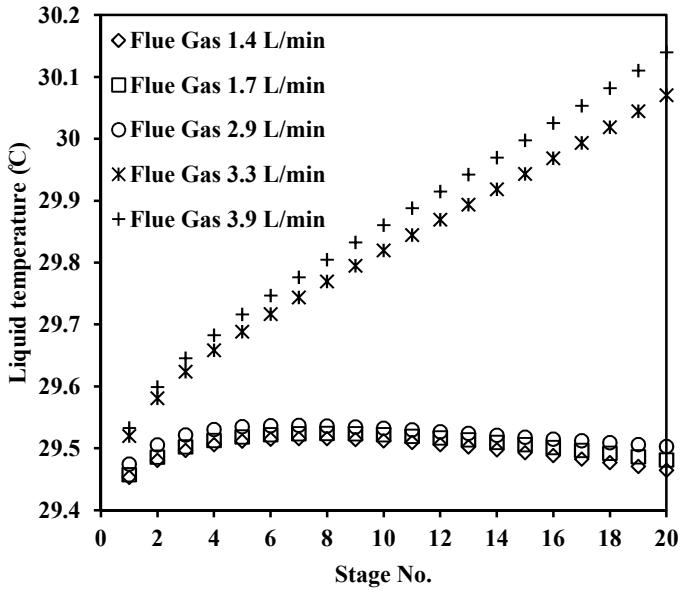

Figure 16. Liquid temperature profiles along the absorber height for different gas flow rates.

Figure 17 indicates the changes in the temperature bulge for different gas flow rates along the absorber height. This figure shows that gas with flow rates of 1.4, 1.7, and 2.9 L/min (Figures a, b, and c) has a temperature bulge at the upper stages of the absorber. The temperature change at the top of the absorber confirms the reaction of CO_2 with solvent and the generation of reaction heat. When the solvent is insufficient compared with the inlet CO_2, the highest absorption will occur at the top of the absorber, causing the temperature bulge there. Heat transfer from liquid to the gas at the lower stages of the column reduces temperature. By increasing the gas flow rate to

3.3 and 3.9 L/min, the temperature bulge broadens along the stages of absorber (Figures d and e). This effect indicates that the heat released from CO_2 absorption is more than the heat consumed for the heating of gas stream. Therefore, the temperature increases along the absorber.

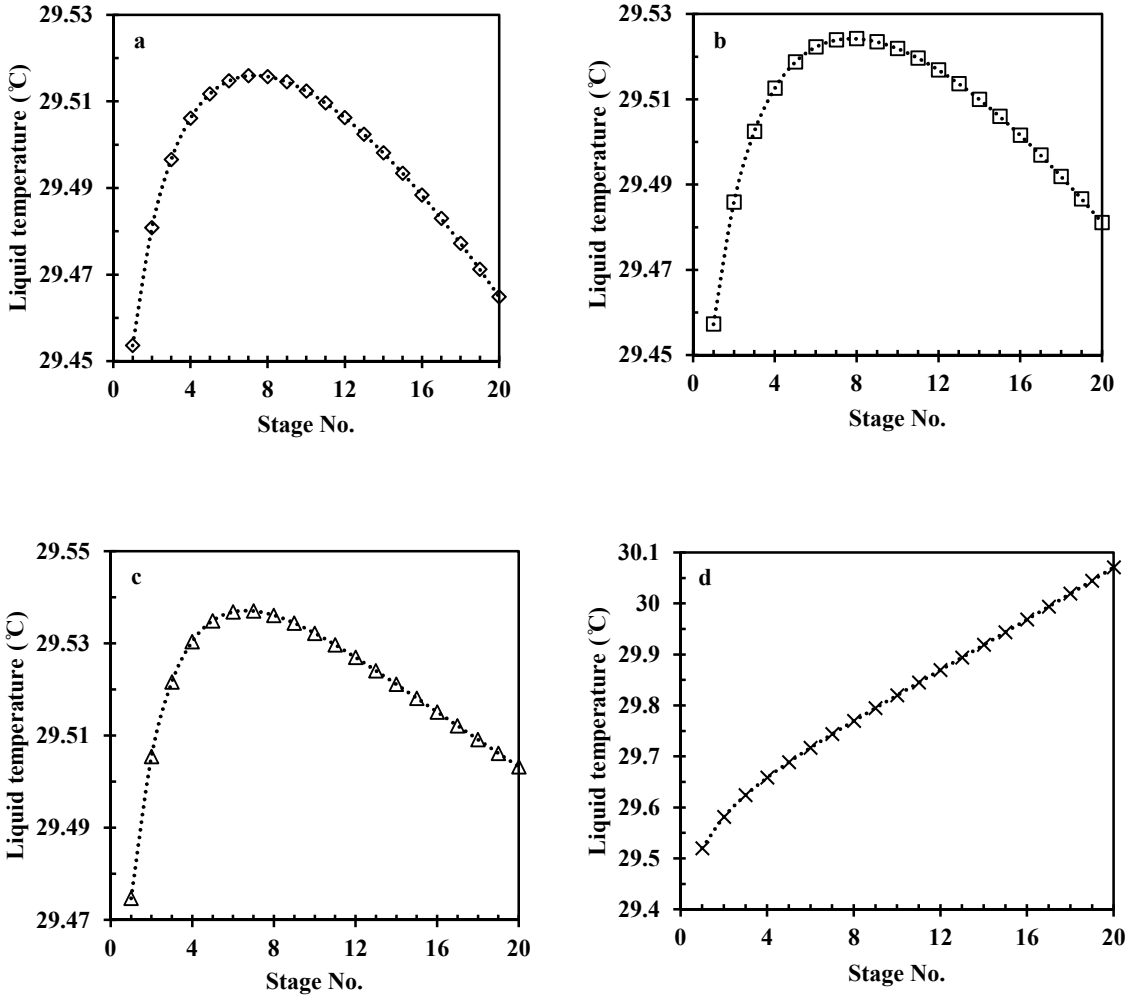

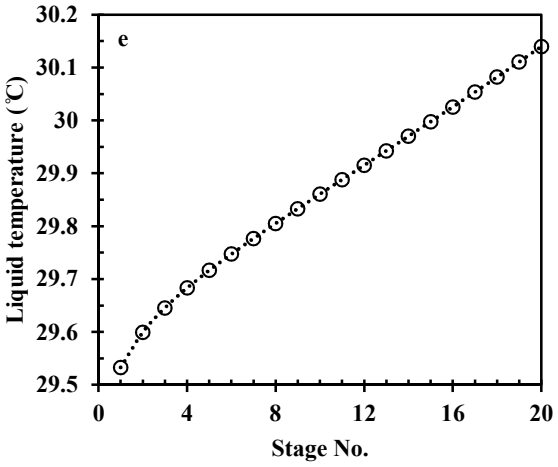

Figure 17. liquid temperature profiles along the absorber height for gas flow rates with a)1.4 L/min b)1.7 L/min c)2.9 L/min d)3.3 L/min e)3.9 L/min.

Table 7 displays the comparison of temperature in the absorber outlet stream between the experimental and simulation studies. In the experimental work, temperature sensors were not installed in the absorption column, and temperature was measured only in the outlet liquid stream. By increasing the gas flow rate from 1.4 L/min to 3.9 L/min, the calculated temperature increases by 2.31% (29.46 °C–30.14 °C). The AAD% value of less than 10% confirms that the simulations match appropriately with the experimental values for all gas flow rates.

Table 7. Rich stream temperature for the CO_2–MEA–glycerol system.

	Temperature (℃)		
Gas flow rate (L/min)	Experimental	Simulation	AAD%
1.4	32.01	29.46	7.96
1.7	32.1	29.48	8.16
2.9	32.21	29.50	9.96
3.3	32.53	30.07	7.56
3.9	32.75	30.14	7.97

Figures 18 and 19 indicate liquid CO_2 mole fraction and CO_2 loadings along the absorption column for different gas flow rates, respectively. The absorber has two feeds: the gas that enters at the bottom of column (stage 20) and flows upward. The MEA–glycerol solvent is fed at the top (stage 1), flowing down the column and contacting the gas phase. During contact between the liquid and the gas phase, the CO_2 enters the liquid phase due to a concentration gradient. MEA drives CO_2 into the liquid phase because of rapid reaction and enhances the absorption rate. CO_2 also dissolves in glycerol solvent without reacting.

As shown in Figures 18 and 19, stages 1 and 20 have the lowest and highest liquid CO_2 mole fraction and CO_2 loadings, respectively. The amount of liquid CO_2 absorption and CO_2 loading increases toward the bottom half of the absorber. When the solvent enters the column at the top,

CO_2 absorption occurs, and CO_2 is transferred to the liquid phase. This liquid phase flows down the absorber. Thus, the amount of absorbed CO_2 on the stages increases toward the bottom of column.

The packings provide contact area for mass transfer. The liquid phase forms a film around the packing, increasing the contact area between the gas and liquid phases. The rich solvent leaves the column in stage 20 and has the highest CO_2 loading.

As can be seen from Figures 18 and 19, by increasing the gas flow rate from 1.4 L/min to 3.9 L/min, the amount of CO_2 increases, and the location of the reaction along the column is transferred to the bottom stages. Thus, CO_2 absorption increases because of the increased driving force, and the reduced amount of CO_2 can transfer to the upper stages. Notably, chemical and physical absorption processes occur on the stages. CO_2 dissolves in the glycerol and flows down the column. When the gas flow rate increases, the amount of CO_2 that can be dissolved in the glycerol increases.

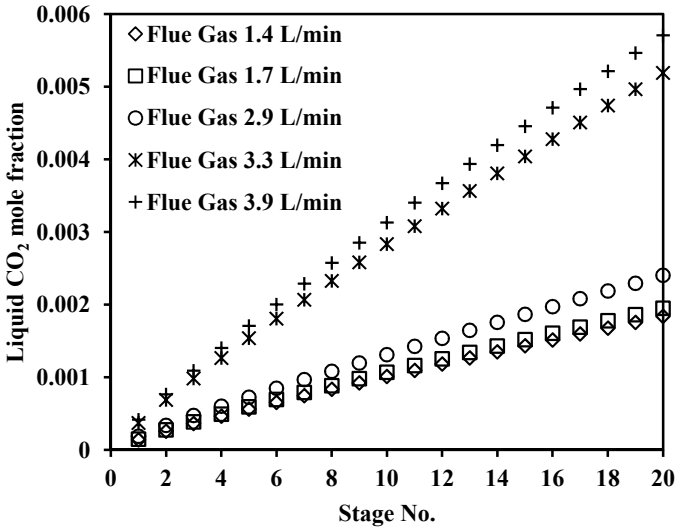

Figure 18. CO_2 mole fraction profiles in liquid phase along the absorption column for the CO_2–MEA–glycerol system.

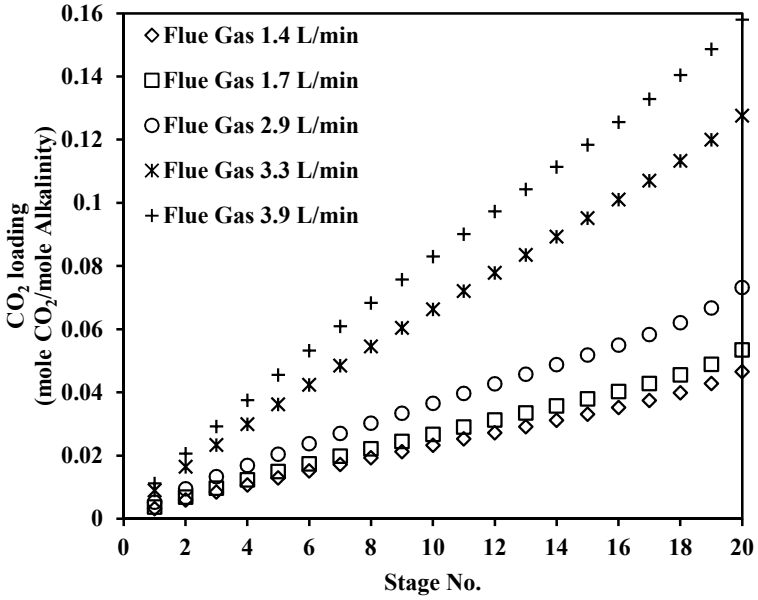

Figure 19. CO_2 loading profiles along the absorption column for the CO_2–MEA–glycerol system.

Figure 20 depicts the effect of the number of stages on CO_2 loading in the absorber column. As shown in the figure, CO_2 loading in the outlet stream from absorber (rich loading) increases when the number of stages is increased. This indicates that although CO_2 removal performance improves, the increase in the number of stages would also increase the capital cost of the equipment. The plot shows that the variation in CO_2 loading in the lower number of stages is more than that in the higher number of stages.

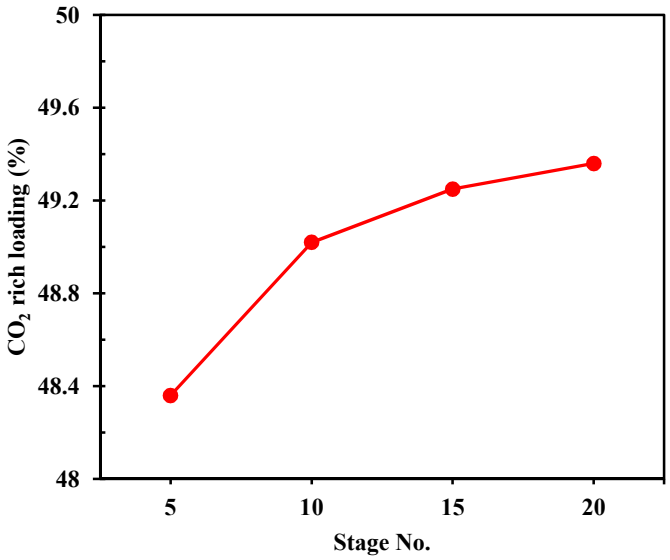

Figure 20. Effect of the number of stages on CO_2 rich loading.

4.2.2. Stripper simulation

The Aspen model was run with 10 mm ceramic Raschig packings. It has a surface area of 4.72 cm^2/cm^3, which is almost similar to the surface area of 8 mm glass Raschig packings (4.61 cm^2/cm^3). This was done because of the convergence problems of the stripper. Different packings with surface areas near 4.61 cm^2/cm^3 were tested in the simulations, and 10 mm ceramic Raschig packings gave the best convergence. Given that only the chemical solvent (MEA) was thermally stripped, this is the only phase that was regenerated at high temperature. However, the physical solvent (glycerol) was regenerated by removing the pressure. Given this operational limitation, the MEA–glycerol solvent was regenerated at 100 °C and 0.1 barg. Therefore, no energy is required to regenerate the glycerol as a physical solvent.[35]

The experimental and simulation results for lean CO_2 loadings at different gas flow rates are compared in Table 8. As shown in the table, by increasing the gas flow rate from 1.4 L/min to 3.9 L/min, lean loading decreases by 13.35% in the simulation. This result indicates an increase

in the reboiler heat duty. The calculated AAD% between experimental and simulated lean loadings is less than 10% for all gas flow rates.

Table 8. CO_2 loadings in outlet stream from the stripper for the CO_2–MEA–glycerol system.

Lean loading (%) (mole CO_2/mole Alkalinity)			
Gas flow rate (L/min)	Experimental	Simulation	AAD%
1.4	4.02	3.67	8.70
1.7	3.89	3.66	5.91
2.9	3.51	3.56	1.42
3.3	3.03	3.33	9.90
3.9	2.96	3.18	7.43

Solvent regeneration occurs when the rich solvent from the absorber enters stage number 2 as the feed of stripper. The regenerated solvent is discharged from stage number 20 while it has low CO_2 loadings.

The rich stream entering stage 2 has the highest CO_2 mole fraction in the column. CO_2 desorption occurs along the stages of desorber, where the chemical reaction of MEA + CO_2 is reversed by the addition of heat. Carbamate reversion (reaction 9) occurs in the desorber column, and the CO_2 is liberated:

$$MEACOO^- + H_3O^+ \rightarrow MEA + H_2O + CO_2 \quad (9)$$

The CO_2-rich solvent needs to be warmed before feeding in the stripper column to decrease the solubility of CO_2 in solvent. The stripper removes CO_2 by increasing the temperature of the solution. The heat produced can drive the mass transfer from the liquid to the gas phase, and the released CO_2 flows upward the column. Therefore, the CO_2 mole fraction in the liquid phase decreases toward the bottom of column.

Figure 21 confirms that reboiler heat duty in the simulation study can be increased by increasing the gas flow rate. The investigation of this figure shows that reboiler heat duty is a function of rich loading. By increasing the gas flow rate from 1.4 L/min to 3.9 L/min, the amount of CO_2 absorption rises in the absorber column. This effect increases the rich loading and the amount of CO_2 to be stripped in the desorber column. Thus, the reboiler heat duty rises by 207.32 Mj/h (98.14–305.46 Mj/h).

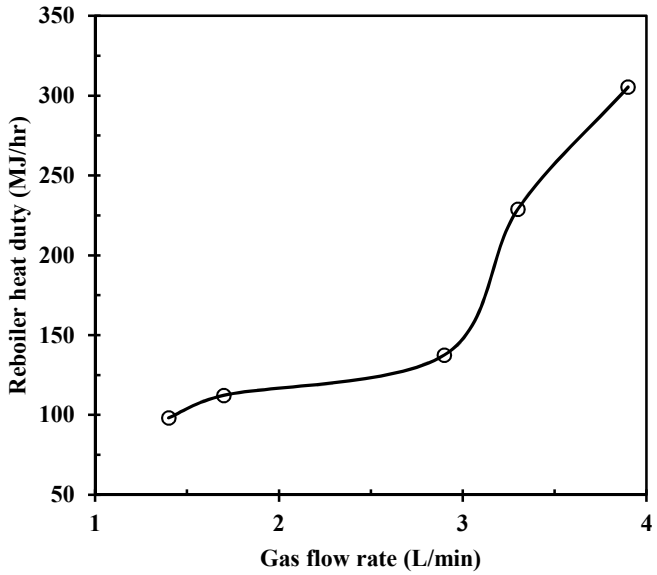

Figure 21. Dependence of the gas flow rate on reboiler heat duty.

Figure 22 demonstrates the CO_2 loading of the lean solvent as a function of the L/G ratio. In this experimental study, the gas flow rate increases in quantities of 1.4, 1.7, 2.9, 3.3, and 3.9 L/min,

whereas the solvent flow rate is kept constant at 0.7 L/min. Accordingly, the ratio of liquid flow rate to gas flow rate (L/G) decreases to 0.5, 0.41, 0.24, 0.21, and 0.18. In Figure 22 experimental and simulation results show that the CO_2 loading decreases as the L/G ratio decreases. This figure confirms that by increasing the gas flow rate, the lean loading decreases. Therefore, reboiler heat duty increases (Figure 21).

As shown in Figure 22, deviation between experimental data and simulation data increased at L/G ratio higher than 0.3. It is mainly due to assumptions considered in modeling as well as mass transfer equations and coefficients used in ASPEN Plus. According to Table 8, the errors for the first three points decreased from 8.70% and 5.91% to 1.42%. Therefore, the trend of diagram is convergent but, for the next two points, the errors increased (9.90% and 7.43%) and the trend of diagram is divergent. The calculated Average absolute deviation percentages (AAD%) between experimental and simulated lean loadings is less than 10% for all gas flow rates (Table 8) and confirmed that the modeling results are reasonably close to the experimental data.

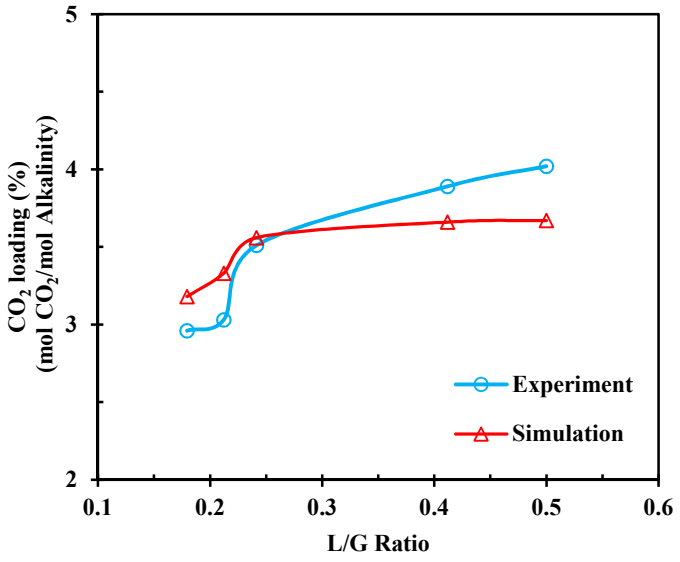

Figure 22. Dependence of the lean CO_2 loading on L/G ratio.

Figure 23 describes the variation in reboiler heat duty with stripper stages. It shows that increasing the stages sharply reduces the reboiler heat duty. However, after this sharp reduction, the reboiler duty seems to decrease slightly for an increased number of stages.

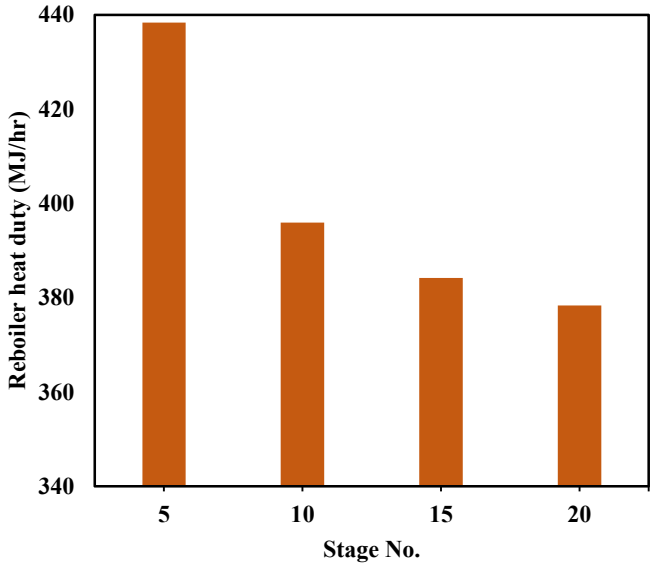

Figure 23. Effect of number of stages on reboiler heat duty.

5. CONCLUSIONS

Experiments were conducted in absorption/desorption unit using aqueous solutions of 10 wt% MEA, 10 wt% glycerol, and 10 wt% MEA–10 wt% glycerol. CO_2-rich loading increased when the gas flow rate increased from 1.4 to 3.9 L/min.

CO_2-rich loading at 1.4 L/min gas flow rate increased from 3.65% mol CO_2/mol MEA to 5.19% mol CO_2/mol alkalinity for MEA-glycerol system. Moreover, CO_2-rich loading at 3.9 L/min gas flow rate increased from 13.9% mol CO_2/mol MEA to 15.96% mol CO_2/mol alkalinity for MEA-glycerol system. Therfore, the hybrid MEA-glycerol solution showed a better CO_2 absorption performance at the specified gas flow rates compared with the MEA system.

An Aspen Plus rate-based model was simulated with five different gas flow rates to the absorber and desorber columns for the 10 wt% MEA–10 wt% glycerol solvent using the ENRTL-RK

thermodynamic model. In all simulations, operating conditions from experiments were used to fit the simulation model. The absorber simulation model predicted the temperature profiles accurately within a deviation percentage in the range of 7%–10% for the experimental and simulated values. In the absorption column, stages 1 and 20 showed the lowest and highest CO_2 loadings, respectively, for all gas flow rates because CO_2 absorption increased toward the bottom half of the column.

The highest deviation percentage between the simulated and experimental values of rich loadings was 9.22% at the gas flow rate of 2.9 L/min. Therefore, the prediction of the simulation model properly matched experimental data.

Five stripper runs with different feed compositions (rich streams) were simulated. The stripper was modeled with a partial-vapor condenser and a kettle reboiler. Reboiler heat duty indicated an increase of 207.32 Mj/h within the gas flow rate range of 1.4 L/min to 3.9 L/min gas, and the deviation percentage between simulated and experimental values for the lean loadings was less than 10% in all five runs.

As a result, post-combustion CO_2 capture using MEA solvent can employ glycerol as promoter to enhance CO_2 absorption capacity.

AUTHOR INFORMATION

Corresponding Author

* E-mail: kheireddinea@sunway.edu.my (M.K. Aroua).

ORCID

Somayeh Mirzaei: 0000-0001-7199-117X

ACKNOWLEDGMENT

This work was performed in the University of Malaya Center for Separation Science and Technology.

ABBREVIATIONS

CO_2, Carbon dioxide; MEA, Monoethanolamine; DEA, diethanolamine; MDEA, N-methyldiethanolamine; PZ, Piperazine; ILs, ionic liquids; PEG, polyethylene glycol; AAD, average absolute deviation.

NOMENCLATURE

$k_{i,k}^{L}$ Binary mass transfer coefficient for the liquid (m/s)

$k_{i,k}^{V}$ Binary mass transfer coefficient for the vapor (m/s)

Re_L Reynolds number for the liquid

Re_V Reynolds number for the vapor

Sc_L Schmidt number for the liquid

Sc_V Schmidt number for the vapor

Fr_L Froude number for the liquid

We_L Weber number for the liquid

Ca_L Capillary number

a_p Specific area of the packing (m^2/m^3)

a_e Effective surface area (m^2/m^3)

a^I Total interfacial area (m^2)

a_w Wetted surface area (m^2/m^3)

A_t Cross-sectional area of the column (m^2)

d_p Nominal packing size (m)

h_p Packed section height (m)

μ_L Liquid viscosity (Pa·s)

ρ_L Liquid density (kg/m^3)

D^V Diffusivity of the vapor (m^2/s)

$\overline{D}^L, \overline{D}^V$ Average diffusivity (m^2/s)

h^L, h^V Heat transfer coefficient (W/ (m^2.K))

$\overline{k}^L, \overline{k}^V$ Average mass transfer coefficient (m/s)

$\bar{\rho}^L, \bar{\rho}^V$ Molar density ($kmol/m^3$)

C_P^L, C_P^V Specific molar heat capacity (J/ (kmol.K))

GREEK LETTERS

g Gravitational constant (m/s^2)

σ Surface tension (N/m)

σ_cCritical surface tension of packing (N/m)

λ Thermal conductivity (W/ (m.K))

REFERENCES

(1) Wu, Z.; Li, W.; Zhu, T.; Zheng, Y.; Wang, T.; Wang, C.; Luo, Y., Investigation of CO_2 absorption kinetics and desorption performance in aqueous 1-(2-Aminoethyl)-3-methylimidazolium bromine solution. *Energy & Fuels* **2018,** 32, (6), 6934-6942.

(2) Wang, L.; Zhang, Y.; Wang, R.; Li, Q.; Zhang, S.; Li, M.; Liu, J.; Chen, B., Advanced monoethanolamine absorption using sulfolane as a phase splitter for CO_2 capture. *Environmental science & technology* **2018,** 52, (24), 14556-14563.

(3) Vitillo, J. G.; Smit, B.; Gagliardi, L., Introduction: Carbon capture and separation. In ACS Publications: 2017.

(4) Guo, H.; Li, H.; Shen, S., CO_2 capture by water-lean amino acid salts: absorption performance and mechanism. *Energy & Fuels* **2018,** 32, (6), 6943-6954.

(5) Babamohammadi, S.; Shamiri, A.; Aroua, M. K., A review of CO_2 capture by absorption in ionic liquid-based solvents. *Reviews in Chemical Engineering* **2015,** 31, (4), 383-412.

(6) Ling, H.; Liu, S.; Wang, T.; Gao, H.; Liang, Z., Characterization and Correlations of CO_2 Absorption Performance into Aqueous Amine Blended Solution of Monoethanolamine (MEA) and N, N-Dimethylethanolamine (DMEA) in a Packed Column. *Energy & Fuels* **2019,** 33, (8), 7614-7625.

(7) Li, L.; Puxty, G.; Maeder, M.; Burns, R.; Yu, H.; Conway, W., Kinetic Absorption of CO_2 into Blended Ammonia (NH_3) Solutions with a New Cyclic Amine 4-Aminomethyltetrahydropyran (4-AMTHP). *Energy & Fuels* **2019,** 33, (6), 5377-5383.

(8) Luo, Q.; Feng, B.; Liu, Z.; Zhou, Q.; Zhang, Y.; Li, N., Experimental Study on Simultaneous Absorption and Desorption of CO_2, SO_2, and NOx Using Aqueous N-

Methyldiethanolamine and Dimethyl Sulfoxide Solutions. *Energy & fuels* **2018,** 32, (3), 3647-3659.

(9) Yusoff, R.; Shamiri, A.; Aroua, M.; Ahmady, A.; Shafeeyan, M.; Lee, W.; Lim, S.; Burhanuddin, S., Physical properties of aqueous mixtures of N-methyldiethanolamine (MDEA) and ionic liquids. *Journal of Industrial and Engineering Chemistry* **2014,** 20, (5), 3349-3355.

(10) Zhang, K.; Hou, Y.; Wang, Y.; Wang, K.; Ren, S.; Wu, W., Efficient and Reversible Absorption of CO_2 by Functional Deep Eutectic Solvents. *Energy & Fuels* **2018,** 32, (7), 7727-7733.

(11) Seo, J.-B.; Jeon, S.-B.; Kim, J.-Y.; Lee, G.-W.; Jung, J.-H.; Oh, K.-J., Vaporization reduction characteristics of aqueous ammonia solutions by the addition of ethylene glycol, glycerol and glycine to the CO_2 absorption process. *Journal of Environmental Sciences* **2012,** 24, (3), 494-498.

(12) Zaman, M.; Lee, J. H., Carbon capture from stationary power generation sources: A review of the current status of the technologies. *Korean Journal of Chemical Engineering* **2013,** 30, (8), 1497-1526.

(13) Sadeghpour, M.; Yusoff, R.; Aroua, M. K., Polymeric ionic liquids (PILs) for CO_2 capture. *Reviews in Chemical Engineering* **2017,** 33, (2), 183-200.

(14) Gurkan, B. E.; Gohndrone, T. R.; McCready, M. J.; Brennecke, J. F., Reaction kinetics of CO_2 absorption in to phosphonium based anion-functionalized ionic liquids. *Physical Chemistry Chemical Physics* **2013,** 15, (20), 7796-7811.

(15) Liu, F.; Fang, M.; Yi, N.; Wang, T., Research on Alkanolamine-Based Physical–Chemical Solutions As Biphasic Solvents for CO_2 Capture. *Energy & Fuels* **2019,** 33, (11), 11389-11398.

(16) Kotamreddy, G.; Hughes, R.; Bhattacharyya, D.; Stolaroff, J.; Hornbostel, K.; Matuszewski, M.; Omell, B., Process Modeling and Techno-Economic Analysis of a CO_2 Capture Process Using Fixed Bed Reactors with a Microencapsulated Solvent. *Energy & Fuels* **2019,** 33, (8), 7534-7549.

(17) Zhao, Y.; Bian, Y.; Li, H.; Guo, H.; Shen, S.; Han, J.; Guo, D., A comparative study of aqueous potassium lysinate and aqueous monoethanolamine for postcombustion CO_2 capture. *Energy & Fuels* **2017,** 31, (12), 14033-14044.

(18) Dugas, R. E., Pilot plant study of carbon dioxide capture by aqueous monoethanolamine. *MSE Thesis, University of Texas at Austin* **2006**.

(19) Wang, M.; Lawal, A.; Stephenson, P.; Sidders, J.; Ramshaw, C., Post-combustion CO_2 capture with chemical absorption: a state-of-the-art review. *Chemical engineering research and design* **2011,** 89, (9), 1609-1624.

(20) Zhang, W.; Jin, X.; Tu, W.; Ma, Q.; Mao, M.; Cui, C., Development of MEA-based CO_2 phase change absorbent. *Applied Energy* **2017,** 195, 316-323.

(21) Wang, R.; Liu, S.; Wang, L.; Li, Q.; Zhang, S.; Chen, B.; Jiang, L.; Zhang, Y., Superior energy-saving splitter in monoethanolamine-based biphasic solvents for CO_2 capture from coal-fired flue gas. *Applied energy* **2019,** 242, 302-310.

(22) Rodrigues, A.; Bordado, J. C.; Santos, R. G. d., Upgrading the glycerol from biodiesel production as a source of energy carriers and chemicals—A technological review for three chemical pathways. *Energies* **2017,** 10, (11), 1817.

(23) Fan, P.; Wang, J.; Xing, S.; Yang, L.; Yang, G.; Fu, J.; Miao, C.; Lv, P., Synthesis of glycerol-free biodiesel with dimethyl carbonate over sulfonated imidazolium ionic liquid. *Energy & Fuels* **2017,** 31, (4), 4090-4095.

(24) Chaves, D. M.; Ferreira, S. O.; Chagas da Silva, R.; Natalino, R.; José da Silva, M. r., Glycerol Esterification over Sn (II)-Exchanged Keggin Heteropoly Salt Catalysts: Effect of Thermal Treatment Temperature. *Energy & Fuels* **2019,** 33, (8), 7705-7716.

(25) Leo, C.; Shamiri, A.; Aroua, M.; Aghamohammadi, N.; Aramesh, R.; Natarajan, E.; Ganesan, P.; Akbari, V., Correlation and measurement of density and viscosity of aqueous mixtures of glycerol and N-methyldiethanolamine, monoethanolamine, piperazine and ionic liquid. *Journal of Molecular Liquids* **2016,** 221, 1155-1161.

(26) Kondawar, S.; Rode, C., Solvent-free glycerol transesterification with propylene carbonate to glycerol carbonate over a solid base catalyst. *Energy & fuels* **2017,** 31, (4), 4361-4371.

(27) Shamiri, A.; Shafeeyan, M.; Tee, H.; Leo, C.; Aroua, M.; Aghamohammadi, N., Absorption of CO_2 into aqueous mixtures of glycerol and monoethanolamine. *Journal of Natural Gas Science and Engineering* **2016,** 35, 605-613.

(28) Jie, G.; Jun, Y.; Feifei, Z.; Xin, C.; Ming, T.; Wanzhong, K.; Yanbo, Z.; Jun, L., Study on absorption and regeneration performance of novel hybrid solutions for CO_2 capture. *Gas* **2016,** 15, (15), 15.

(29) Mirzaei, S.; Shamiri, A.; Aroua, M. K., A review of different solvents, mass transfer, and hydrodynamics for postcombustion CO_2 capture. *Reviews in Chemical Engineering* **2015,** 31, (6), 521-561.

(30) Hsu, Y.-H.; Leron, R. B.; Li, M.-H., Solubility of carbon dioxide in aqueous mixtures of (reline+ monoethanolamine) at T=(313.2 to 353.2) K. *The Journal of Chemical Thermodynamics* **2014,** 72, 94-99.

(31) Zhai, R.; Yu, H.; Feng, L.; Chen, Y.; Li, K.; Yang, Y., Integration of a Coal-Fired Power Plant with an Ammonia-Based CO_2 Capture Process in Three Operation Modes. *Energy & fuels* **2018,** 32, (10), 10760-10772.

(32) Mirzaei, S.; Shamiri, A.; Aroua, M. K., Simulation of aqueous blend of monoethanolamine and glycerol for carbon dioxide capture from flue gas. *Energy & Fuels* **2016,** 30, (11), 9540-9553.

(33) Hajari, A.; Atanga, M.; Hartvigsen, J. L.; Rownaghi, A. A.; Rezaei, F., Combined Flue Gas Cleanup Process for Simultaneous Removal of SOx, NOx, and CO_2, A Techno-Economic Analysis. *Energy & Fuels* **2017,** 31, (4), 4165-4172.

(34) Wang, T., Degradation of aqueous 2-Amino-2-methyl-1-propanol for carbon dioxide capture. **2013**.

(35) Kingma, A. Understanding the equilibrium behaviour of a novel phase splitting solvent in the presence of high pressure CO_2. 2016.

(36) Burr, B.; Lyddon, L. In *A comparison of physical solvents for acid gas removal*, Gas Processors' Association Convention, Grapevine, TX, 2008; 2008.

(37) Babamohammadi, S.; Shamiri, A.; Borhani, T. N. G.; Shafeeyan, M. S.; Aroua, M. K.; Yusoff, R., Solubility of CO_2 in aqueous solutions of glycerol and monoethanolamine. *Journal of Molecular Liquids* **2018,** 249, 40-52.

(38) Domínguez-Barroso, V.; Herrera, C.; Larrubia, M. Á.; Alemany, L. J., Coupling of glycerol-APR and in situ hydrodeoxygenation of fatty acid to produce hydrocarbons. *Fuel processing technology* **2019,** 190, 21-28.

(39) Medina-Gonzalez, Y.; Tassaing, T.; Camy, S.; Condoret, J.-S., Phase equilibrium of the CO_2/glycerol system: Experimental data by in situ FT-IR spectroscopy and thermodynamic modeling. *The Journal of Supercritical Fluids* **2013,** 73, 97-107.

(40) Oğuz, H.; Öztürk, S.; Alper, E., Meassument of Effective Interfacial Area In A Packed-Column Absorher By Sulphite Oxidation Method: Influence of Liquid Viscosity.

(41) Baker, M., Inc. , Environmental Health & Safety. MSDS Number G4774,U.S.

(42) Dugas, R. E., Rate and Equilibrium Measurements of MEA/Piperazine. *Methods* **2007,** 2, (2).

(43) Zhao, J.; Song, X.; Sun, Z.; Yu, J., Simulation on thermodynamic state of ammonia carbonation at low temperature and low pressure. *Frontiers of Chemical Science and Engineering* **2013,** 7, (4), 447-455.

(44) Bravo, J. L.; Fair, J. R., Generalized correlation for mass transfer in packed distillation columns. *Industrial & Engineering Chemistry Process Design and Development* **1982,** 21, (1), 162-170.

(45) Aspen Technology, Aspen Plus help file, Burlington, MA, USA **2011**.

(46) Chilton, T. H.; Colburn, A. P., Mass transfer (absorption) coefficients prediction from data on heat transfer and fluid friction. *Industrial & engineering chemistry* **1934,** 26, (11), 1183-1187.

(47) Onda, K.; Takeuchi, H.; Okumoto, Y., Mass transfer coefficients between gas and liquid phases in packed columns. *Journal of chemical engineering of Japan* **1968,** 1, (1), 56-62.

(48) Stewart, W. E., Multicomponent mass transfer. By Ross Taylor and R. Krishna, Wiley, New York, 1993, 579 pp. *AIChE Journal* **1995,** 41, (1), 202-203.